THE JOURNAL OF PHYSICAL CHEMISTRY Letters

Letter

pubs.acs.org/JPCL

An Optocatalytic Model for Semiconductor–Catalyst Water-Splitting Photoelectrodes Based on In Situ Optical Measurements on Operational Catalysts

Lena Trotochaud, Thomas J. Mills, and Shannon W. Boettcher*

Department of Chemistry and the Center for Sustainable Materials Chemistry, University of Oregon, Eugene, Oregon 97403, United States

Supporting Information

ABSTRACT: The optical properties of electrocatalysts are important for photoelectrochemical water splitting because colored catalysts on the surface of semiconductor photoelectrodes parasitically absorb photons and lower the system efficiency. We present a model that describes the coupling of colored oxygen evolution reaction (OER) electrocatalyst thin films with semiconductor photoelectrodes. We use this model to define an "optocatalytic" efficiency ($\Phi_{o\text{-}c}$) based on experimental optical and electrokinetic data collected in basic solution. Because transition-metal oxides, hydroxides, and oxyhydroxides often exhibit electrochromism, in situ spectroelectrochemistry is used to quantify the optical absorption of active NiO_x, CoO_x, $NiCoO_x$, $Ni_{0.9}Fe_{0.1}O_x$, and IrO_x catalyst films at OER potentials. For the highest-activity $Ni_{0.9}Fe_{0.1}O_x$ catalyst, $\Phi_{o\text{-}c}$ is maximized (0.64) for a thickness of ∼0.4 nm (∼2 monolayers). This work quantitatively shows that ultrathin catalyst films are appropriate to optimize the performance of water-splitting photoelectrodes and thus assists in the design and study of efficient photoelectrochemical water-splitting devices.

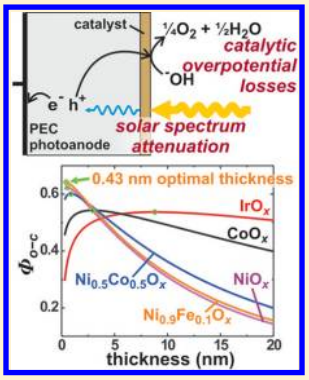

SECTION: Energy Conversion and Storage; Energy and Charge Transport

Photochemical water electrolysis to form hydrogen and oxygen gas (i.e., solar water splitting, $H_2O \rightarrow H_2 + 1/2O_2$) provides a pathway for the large-scale conversion and storage of solar energy.[1,2] Water-splitting photoelectrochemical (PEC) cells typically consist of at least two classes of materials, (1) inorganic semiconductors or molecular chromophores that absorb sunlight to generate excited electron–hole pairs and (2) electrocatalysts that facilitate the fuel-forming hydrogen and oxygen evolution reactions (HER and OER, respectively).[1] In particular, the OER (e.g., $4OH^- \rightarrow 2H_2O + O_2 + 4e^-$ in basic media) is kinetically slow and a significant source of efficiency loss in both electrically driven and photodriven water electrolysis.[2,3]

The separate optimization and development of materials for either semiconductor photoelectrodes or electrocatalysts has been studied for several decades.[1,4,5] Recently, significant effort has been extended to incorporate OER catalysts with semiconductor photoanodes and understand the response of the composite systems.[5−22] The optical properties of the catalyst layer affect the light absorption of the underlying semiconductor substrate but have not been quantitatively addressed. Furthermore, the transition-metal oxides, hydroxides, and oxyhydroxides used as OER electrocatalysts often exhibit electrochromism (and thus have applications also in "smart" windows[23,24]). The optical properties of these catalysts measured in the resting state are therefore expected to differ from those measured at operational potentials. Because of the trade-off between increased parasitic optical absorption and decreased overpotential as the film thickness is increased,[21] quantitative evaluation of the underlying optical, catalytic, and semiconductor device processes is important for uncovering the design principles governing the performance of composite photoelectrode systems.[25]

We present a model for composite PEC current–potential response that includes both catalytic and optical measurements made in situ during oxygen evolution for a range of electrocatalyst materials. Recently, we reported the solution synthesis and catalytic activities of several OER electrocatalyst thin-film materials, including NiO_x, $NiCoO_x$, CoO_x, IrO_x, and $Ni_{0.9}Fe_{0.1}O_x$, which we found had the highest activity of any OER electrocatalyst in basic media.[26] Here, we report the quantitative analysis of the optical properties of these thin films under OER conditions using in situ spectroelectrochemistry. The combined electrokinetic and in situ optical absorption data are used to define an "optocatalytic" efficiency ($\Phi_{o\text{-}c}$). $\Phi_{o\text{-}c}$ is a function of catalyst loading. At optimal catalyst loading, $\Phi_{o\text{-}c}$ is a quantitative measure of the utility of a particular electrocatalyst for composite semiconductor–catalyst PEC water-splitting systems.

Complete experimental details can be found in the Supporting Information. For optical measurements, catalysts were deposited onto ITO-coated glass substrates from ethanolic solutions of metal salts containing surfactant to

Received: February 4, 2013
Accepted: March 6, 2013
Published: March 6, 2013

decrease surface tension and promote even film coverage.[26] Annealing at 300 °C for 5 min resulted in ∼2 nm films with uniform coverage across the surface of the substrates. All films containing Ni were electrochemically conditioned in 1 M KOH by applying 10 mA cm^{-2} (anodic) for 6 h prior to optical measurements. This conditioning process converts the Ni-containing oxides to oxyhydroxides that are the active catalyst materials.[26] In situ optical experiments were performed in a spectroelectrochemical cell (Figure S1, Supporting Information). The optical transmission spectra of the conditioned films were measured at constant applied potentials after waiting 30 s to reach steady state. Figure 1A shows a cyclic voltammogram

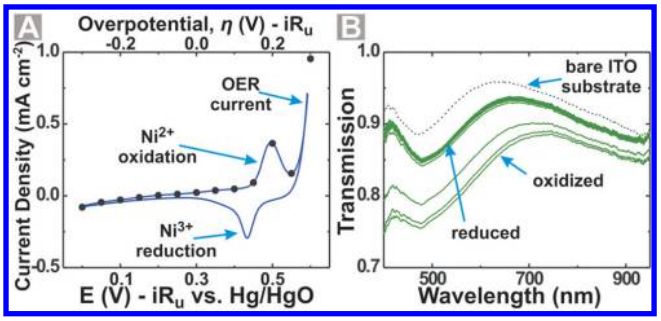

Figure 1. (A) CV of a NiO_x film on ITO collected in the spectroelectrochemical cell. The points on the CV indicate the potentials where steady-state optical measurements were made. The CV was collected in 1 M KOH at 20 mV s^{-1}. (B) UV−vis transmission spectra of a conditioned NiO_x film held at constant potentials. Thirteen spectra are shown for the NiO_x film, each taken at 0.05 V intervals starting at 0 V and increasing to 0.6 V versus Hg/HgO.

(CV) along with the potentials used for the steady-state measurements. Figure 1B shows each transmission spectrum collected from 0.0−0.60 V versus Hg/HgO in 0.05 V increments. The transmission remains constant until ∼0.5 V versus Hg/HgO, which is near the peak of the oxidation wave (nominally Ni^{2+}/Ni^{3+}). This behavior is consistent with previous studies of electrochromism in NiO_x and $Ni(OH)_2$.[27−29]

Figure 2 shows the transmission spectra for NiO_x, $NiCoO_x$, CoO_x, $Ni_{0.9}Fe_{0.1}O_x$, and IrO_x thin films in the resting (reduced) and catalytically active (oxidized) states. Spectra for the resting film states were collected at 0 V applied versus Hg/HgO. Spectra for the active states were collected at 1 mA cm^{-2}

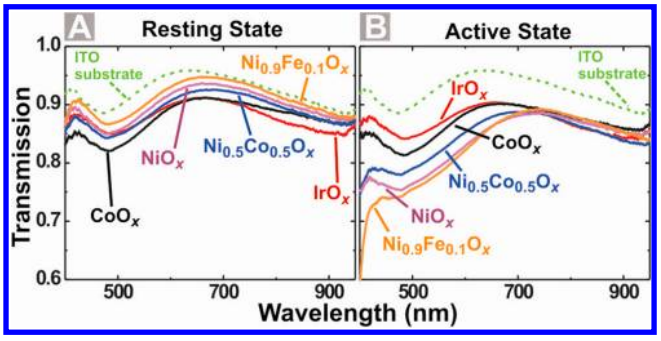

Figure 2. In situ spectroelectrochemical measurements of resting (A) and active (B) catalyst films. The dashed line shows the transmission spectrum of the ITO substrate. The catalyst spectra shown are not corrected for reflection or absorption of the ITO substrate. The cuvette filled with electrolyte was used as a blank for the measurement.

applied anodic current. This current density was sufficient to oxidize the films to their active state without generating visible bubbles at the electrode surface. At higher currents where small bubbles were visible, the transmission spectra did not significantly change. Only samples containing Ni displayed a significant difference in optical transmission between the resting and active catalyst. For all of the Ni-containing films, optical switching between the active and resting states correlated with the positions of the Ni^{2+}/Ni^{3+} oxidation and reduction waves, respectively, in the voltammetry. The electrochromic response is completely reversible upon cycling, which is not always observed in thicker films.[29]

The measured optical and electrokinetic data were used to predict how changing the thickness of the catalyst films would affect the photocurrent and photovoltage at maximum power for a composite photoelectrode. Figure 3 shows a schematic of

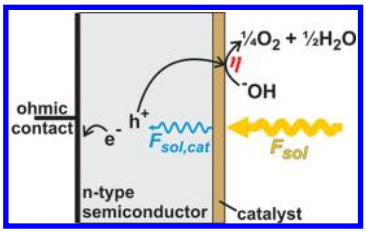

Figure 3. A composite PEC photoanode where the catalyst thin film attenuates the solar flux that reaches the semiconductor photoelectrode.

the composite photoelectrode considered. The relevant input parameters depend on the material properties. For example, if the catalyst is on n-Fe_2O_3 with a band gap of E_g = 2.2 eV, only photons with $\lambda \leq 560$ nm are absorbed in the semiconductor. As an example, we analyze an n-type photoanode with E_g = 1.8 eV ($\lambda \leq 690$ nm). Under 1 sun illumination and in the absence of catalyst optical absorption, we choose an initial short-circuit photocurrent $J_{ph,i}$ = 10 mA cm^{-2} and a dark saturation current $J_o = 6.8 \times 10^{-23}$ A cm^{-2} such that the photoelectrode outputs an open-circuit voltage V_{oc} = 1.2 V based on the ideal diode equation (see below). These parameters represent those suitable for an efficient photoanode component of a tandem PEC water-splitting device.[1] The photovoltage output is referenced to the reversible potential for the water oxidation reaction $E(O_2/OH^-)$, meaning that the photocurrent onset potential would be at +0.03 V versus the reversible hydrogen electrode (RHE). For simplicity, we assume that J_o of the bare photoanode is not modified by the addition of a catalyst layer. This implies that the semiconductor and catalysis processes occur in series and that the semiconductor Fermi level is pinned at the surface (for instance, by the catalyst or via a buried semiconductor junction). This model therefore does not include changes to interface band-bending or surface recombination rates with the addition of the catalyst, which appear to be important for some materials systems such as Fe_2O_3/Co−Pi.[6]

In a composite PEC, as shown in Figure 3, the catalyst determines the magnitude of both the photocurrent loss due to parasitic optical absorption and the photovoltage loss due to the kinetic overpotential. To model the parasitic optical absorption of the catalyst, the optical absorption of the catalyst layer, corrected for reflection and absorption by the ITO substrate, is needed. We extract the wavelength-dependent absorption probability of a photon that reaches the catalyst, a_c,

dx.doi.org/10.1021/jz4002604 | J. Phys. Chem. Lett. 2013, 4, 931−935

by accounting for the absorption and reflection at each film and interface, respectively, in the experiment cell (see the Supporting Information for details). Reflection spectra were collected independently using an integrating sphere. The transmission probability for photons entering the catalyst layer is then $T_c(\lambda) = 1 - a_c(\lambda)$. The wavelength-dependent effective absorption coefficient $\alpha(\lambda)$ of the catalyst is given by

$$\alpha(\lambda) = \frac{-\ln(T_c(\lambda))}{t_o} \quad (1)$$

where $\alpha(\lambda)$ has units of cm^{-1} and t_o is the effective film thickness obtained for each film using quartz crystal microgravimetry and the catalyst density.[26] The calculated values of $\alpha(\lambda)$ for the different catalyst thin films are shown in Figure 4A.

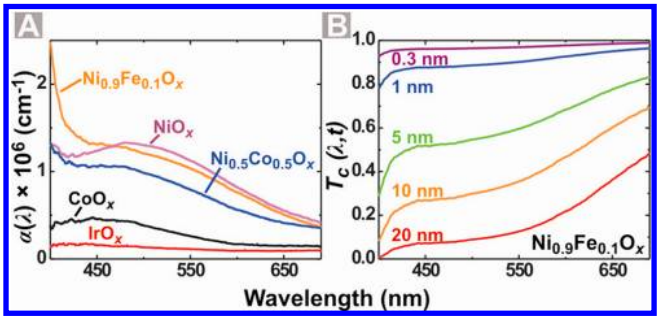

Figure 4. (A) Effective absorption coefficient $\alpha(\lambda)$ calculated for the active catalyst films. (B) Predicted transmission probabilities $T_c(\lambda)$ for $Ni_{0.9}Fe_{0.1}O_x$ films of varying thickness t.

The predicted optical transmission T_c through the catalyst is then a function of the film thickness t, as shown in Figure 4B for the $Ni_{0.9}Fe_{0.1}O_x$ film. The solar flux incident on the semiconductor surface that is transmitted through the catalyst thin film $F_{sol,cat}(\lambda,t)$ is given by

$$F_{sol,cat}(\lambda, t) = F_{sol}(\lambda)T_c(\lambda, t) \quad (2)$$

where $F_{sol}(\lambda)$ is the solar flux defined by the ASTM AM 1.5 standard. We define the catalyst optical efficiency $\varphi_{opt}(t)$ as

$$\varphi_{opt}(t) = \frac{\int_{\lambda_1}^{\lambda_2} F_{sol,cat}(\lambda, t)\, d\lambda}{\int_{\lambda_1}^{\lambda_2} F_{sol}(\lambda)\, d\lambda} \quad (3)$$

where $F_{sol}(\lambda)$ and $F_{sol,cat}(\lambda,t)$ are integrated over the wavelength range relevant for the underlying semiconductor for a catalyst film of thickness t. Here, λ_1 is 400 nm and is determined by the spectrometer range, and λ_2 is 690 nm, the threshold for absorption in the 1.8 eV band gap photoanode under consideration.

Figure 5A shows $\varphi_{opt}(t)$ for varying film thicknesses. Relevant photocurrent losses occur even for films thinner than 10 nm. $\varphi_{opt}(t)$ is incorporated into the ideal photodiode equation to account for the catalyst optical properties in the composite photoelectrode current−voltage (J−V) response

$$J = \varphi_{opt}(t)J_{ph,i} - J_o\left(\exp\left(-\frac{qV_{diode}}{nkT}\right) - 1\right) \quad (4)$$

where J is the total current, J_o is the dark saturation current, V_{diode} is the voltage dropped across the photodiode (i.e., the difference in the quasi-Fermi level in the semiconductor bulk and the catalyst layer), q is the elementary charge, n is the diode

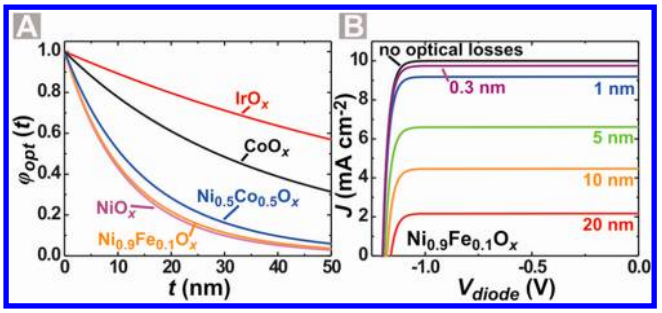

Figure 5. (A) Optical efficiency $\varphi_{opt}(t)$ calculated from eq 3 for the catalysts as a function of film thickness t. (B) Calculated photoelectrode J−V curves using eq 4 for the $Ni_{0.9}Fe_{0.1}O_x$ catalyst in the absence of kinetic overpotentials. The potential is referenced to $E(O_2/OH^-) \equiv 0$ V on this scale. The photovoltage is negative for an n-type photoanode relative to $E(O_2/OH^-)$, based on the electrochemical convention.

ideality factor (assumed $n = 1$), k is Boltzmann's constant, and T is temperature (300 K). For $Ni_{0.9}Fe_{0.1}O_x$, the J−V responses for different catalyst thicknesses (t = 0.3−20 nm) are shown in Figure 5B.

There will also be a voltage drop due to the catalytic overpotential η for driving oxygen evolution. We define η as a function of film thickness t, assuming that the number of active sites increases linearly with film loading, leading to a linear increase in current with film mass at a given η. This is appropriate for porous or ion-permeable films,[26] for example, NiOOH or CoOOH, where such activity scaling has been observed.[30,31] Because the steady-state electrokinetic data[26] are not completely linear on a semilog "Tafel" plot, they were fit to third-order polynomial functions

$$\eta(t, J) = A\log\left(\frac{J}{t}\right)^3 + B\log\left(\frac{J}{t}\right)^2 + C\log\left(\frac{J}{t}\right) + D \quad (5)$$

where, here, J is the current density that the catalyst is required to pass and A, B, C, and D are constants determined by the polynomial fit.

The total voltage across the photoelectrode accounting for η is $V_{total} = V_{diode} + \eta$. Rearranging eq 4 to incorporate η yields

$$V_{total} = -\frac{nkT}{q}\ln\left(\frac{\varphi_{opt}(t)J_{ph,i} - J}{J_o} + 1\right) + \eta(t, J) \quad (6)$$

The steady-state electrokinetic data and polynomial fits are shown in Figure 6A. Current−voltage curves for the $Ni_{0.9}Fe_{0.1}O_x$ catalyst of varying thickness (t = 0.3−20 nm) calculated using eq 6 are shown in Figure 6B.

Figure 6B shows that each catalyst thickness has a different maximum power output P_{max}. The maximum power output of the photoelectrode in the absence of optical and kinetic losses (i.e., no catalyst) $P_{o,max}$ is 10.8 mW cm^{-2} (V = −1.10 V; J = 9.77 mA cm^{-2}). The optocatalytic efficiency, $\Phi_{o\text{-}c}$ is

$$\Phi_{o\text{-}c} = \frac{P_{max}}{P_{o,max}} \quad (7)$$

where P_{max} is the maximum power of the composite photoelectrode. $\Phi_{o\text{-}c}$ is the relevant figure-of-merit for catalyst performance.[32] The maximum values of $\Phi_{o\text{-}c}$ as a function of thickness are labeled in Figure 7. For the most active Ni-based catalysts, $\Phi_{o\text{-}c}$ is maximized for subnanometer catalyst loading, that is, only about two monolayers.

dx.doi.org/10.1021/jz4002604 | J. Phys. Chem. Lett. 2013, 4, 931−935

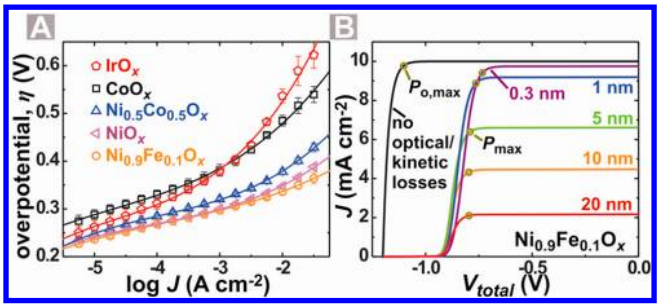

Figure 6. (A) Steady-state electrokinetic data (points) and corresponding polynomial fits (lines) for the catalyst thin films (data from ref 26). (B) Photoelectrode current−voltage curves calculated using eq 6 for the $Ni_{0.9}Fe_{0.1}O_x$ catalyst as an example. The potential is referenced to $E(O_2/OH^-) \equiv 0$ V on this scale. The n-type photoanode produces a photovoltage and photocurrent due to water oxidation at potentials negative (cathodic) of $E(O_2/OH^-)$, thus converting solar energy to stored chemical energy. The maximum power point is calculated based on the photovoltage shift from $E(O_2/OH^-)$. For a complete discussion of these definitions, see ref 1.

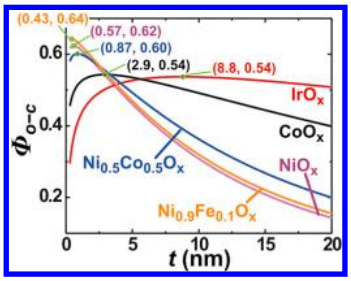

Figure 7. Optocatalytic efficiency $\Phi_{o\text{-}c}$ plots for the catalysts as a function of film thickness, t.

This result can be explained as follows. The kinetic loss η decreases roughly as the log of the film thickness. For example, with a Tafel slope of 30 mV dec^{-1}, a 10-fold increase in catalyst thickness reduces the voltage loss by 30 mV. However, in the thin limit (where the total optical absorption by the catalyst is small), a 10-fold increase in film thickness will lead to roughly a 10-fold increase in optical loss. Furthermore, any decreased J_{ph} associated with increased catalyst loading decreases the photovoltage output of the semiconductor based on eq 6. These factors combine to drive the optimal catalyst loadings to ultrathin films, where the optical losses are low (i.e., less than ~10%). The highly absorbing, but highly active, Ni-based catalysts show a precipitous drop in $\Phi_{o\text{-}c}$ after the optimal film thickness. For the less active but more transparent films such as IrO_x, the peak in $\Phi_{o\text{-}c}$ is broad and lower than that of the $Ni_{0.9}Fe_{0.1}O_x$. This analysis therefore quantitatively shows that very low loadings of active catalysts, even when highly colored, yield the highest-efficiency photoanodes.

In conclusion, we have quantified the effects of parasitic catalyst optical absorption and overpotential losses on the efficiency and measurable photoresponse characteristics of composite semiconductor−catalyst systems. We defined a new efficiency figure-of-merit $\Phi_{o\text{-}c}$ that accounts for both optical and voltage efficiency terms, which are both important for applications in photoelectrochemical water splitting. Maximizing $\Phi_{o\text{-}c}$ led to an optimal film thickness that was subnanometer for the most-active Ni-based catalysts. This simple model can be used to evaluate arbitrary catalyst−semiconductor combinations and determine the relative utility of catalysts with a range of optical properties and activities. The results reported here should therefore assist in the design and study of composite catalyst−semiconductor photoelectrodes.

■ ASSOCIATED CONTENT

Supporting Information

Experimental details, Figure S1, optical model to extract a_c, sample reflection measurements and methods. This material is available free of charge via the Internet at http://pubs.acs.org.

■ AUTHOR INFORMATION

Corresponding Author

*E-mail: swb@uoregon.edu.

Notes

The authors declare no competing financial interest.

■ ACKNOWLEDGMENTS

L.T. and the synthesis/optical characterization of thin-film electrocatalysts were supported by the National Science Foundation under the Centers for Chemical Innovation Program, Grant CHE-1102637. T.J.M. and the theoretical development of the optocatalytic model were supported by the DOE Basic Energy Sciences grant DE-FG02-12ER16323. S.W.B. acknowledges support from the DuPont Young Professor Program. We thank the UO Machine Shop for assistance with construction of a sample holder for reflection measurements, Mark Lonergan for use of the UV−vis spectrometer, and George Nazin for discussions regarding the optical model.

■ REFERENCES

(1) Walter, M. G.; Warren, E. L.; McKone, J. R.; Boettcher, S. W.; Mi, Q.; Santori, E. A.; Lewis, N. S. Solar Water Splitting Cells. *Chem. Rev.* **2010**, *110*, 6446−6473.

(2) Cook, T. R.; Dogutan, D. K.; Reece, S. Y.; Surendranath, Y.; Teets, T. S.; Nocera, D. G. Solar Energy Supply and Storage for the Legacy and Nonlegacy Worlds. *Chem. Rev.* **2010**, *110*, 6474−6502.

(3) Suntivich, J.; May, K. J.; Gasteiger, H. A.; Goodenough, J. B.; Shao-Horn, Y. A Perovskite Oxide Optimized for Oxygen Evolution Catalysis from Molecular Orbital Principles. *Science* **2011**, *334*, 1383−1385.

(4) Tran, P. D.; Wong, L. H.; Barber, J.; Loo, J. S. C. Recent Advances in Hybrid Photocatalysts for Solar Fuel Production. *Energy Environ. Sci.* **2012**, *5*, 5902−5918.

(5) Sun, J.; Zhong, D. K.; Gamelin, D. R. Composite Photoanodes for Photoelectrochemical Solar Water Splitting. *Energy Environ. Sci.* **2010**, *3*, 1252−1261.

(6) Klahr, B.; Gimenez, S.; Fabregat-Santiago, F.; Bisquert, J.; Hamann, T. W. Photoelectrochemical and Impedance Spectroscopic Investigation of Water Oxidation with "Co−Pi"-Coated Hematite Electrodes. *J. Am. Chem. Soc.* **2012**, *134*, 16693−16700.

(7) Seabold, J. A.; Choi, K.-S. Effect of a Cobalt-Based Oxygen Evolution Catalyst on the Stability and the Selectivity of Photo-Oxidation Reactions of a WO_3 Photoanode. *Chem. Mater.* **2011**, *23*, 1105−1112.

(8) Liu, R.; Lin, Y.; Chou, L.-Y.; Sheehan, S. W.; He, W.; Zhang, F.; Hou, H. J. M.; Wang, D. Water Splitting by Tungsten Oxide Prepared by Atomic Layer Deposition and Decorated with an Oxygen-Evolving Catalyst. *Angew. Chem., Int. Ed.* **2011**, *50*, 499−502.

(9) Kay, A.; Cesar, I.; Grätzel, M. New Benchmark for Water Photooxidation by Nanostructured α-Fe_2O_3 Films. *J. Am. Chem. Soc.* **2006**, *128*, 15714−15721.

(10) Tilley, S. D.; Cornuz, M.; Sivula, K.; Grätzel, M. Light-Induced Water Splitting with Hematite: Improved Nanostructure and Iridium Oxide Catalysis. *Angew. Chem., Int. Ed.* **2010**, *49*, 6405−6408.

(11) Abdi, F. F.; van de Krol, R. Nature and Light Dependence of Bulk Recombination in Co-Pi-Catalyzed $BiVO_4$ Photoanodes. *J. Phys. Chem. C* **2012**, *116*, 9398−9404.
(12) Gamelin, D. R. Water Splitting: Catalyst or Spectator? *Nat. Chem.* **2012**, *4*, 965−967.
(13) Zhong, D. K.; Gamelin, D. R. Photoelectrochemical Water Oxidation by Cobalt Catalyst ("Co-Pi")/α-Fe_2O_3 Composite Photoanodes: Oxygen Evolution and Resolution of a Kinetic Bottleneck. *J. Am. Chem. Soc.* **2010**, *132*, 4202−4207.
(14) Ye, H.; Park, H. S.; Bard, A. J. Screening of Electrocatalysts for Photoelectrochemical Water Oxidation on W-Doped $BiVO_4$ Photocatalysts by Scanning Electrochemical Microscopy. *J. Phys. Chem. C* **2011**, *115*, 12464−12470.
(15) Zhong, D. K.; Choi, S.; Gamelin, D. R. Near-Complete Suppression of Surface Recombination in Solar Photoelectrolysis by "Co-Pi" Catalyst-Modified W:$BiVO_4$. *J. Am. Chem. Soc.* **2011**, *133*, 18370−18377.
(16) McDonald, K. J.; Choi, K.-S. Photodeposition of Co-Based Oxygen Evolution Catalysts on α-Fe_2O_3 Photoanodes. *Chem. Mater.* **2011**, *23*, 1686−1693.
(17) Barroso, M.; Cowan, A. J.; Pendlebury, S. R.; Grätzel, M.; Klug, D. R.; Durrant, J. R. The Role of Cobalt Phosphate in Enhancing the Photocatalytic Activity of α-Fe_2O_3 toward Water Oxidation. *J. Am. Chem. Soc.* **2011**, *133*, 14868−14871.
(18) Steinmiller, E. M. P.; Choi, K.-S. Photochemical Deposition of Cobalt-Based Oxygen Evolving Catalyst on a Semiconductor Photoanode for Solar Oxygen Production. *Proc. Natl. Acad. Sci. U.S.A.* **2009**, *106*, 20633−20636.
(19) Surendranath, Y.; Bediako, D. K.; Nocera, D. G. Interplay of Oxygen-Evolution Kinetics and Photovoltaic Power Curves on the Construction of Artificial Leaves. *Proc. Natl. Acad. Sci. U.S.A.* **2012**, *109*, 15617−15621.
(20) Pijpers, J. J. H.; Winkler, M. T.; Surendranath, Y.; Buonassisi, T.; Nocera, D. G. Light-Induced Water Oxidation at Silicon Electrodes Functionalized with a Cobalt Oxygen-Evolving Catalyst. *Proc. Natl. Acad. Sci. U.S.A.* **2011**, *108*, 10056−10061.
(21) Reece, S. Y.; Hamel, J. A.; Sung, K.; Jarvi, T. D.; Esswein, A. J.; Pijpers, J. J. H.; Nocera, D. G. Wireless Solar Water Splitting Using Silicon-Based Semiconductors and Earth-Abundant Catalysts. *Science* **2011**, *334*, 645−648.
(22) Young, E. R.; Costi, R.; Paydavosi, S.; Nocera, D. G.; Bulović, V. Photo-Assisted Water Oxidation with Cobalt-Based Catalyst Formed from Thin-Film Cobalt Metal on Silicon Photoanodes. *Energy Environ. Sci.* **2011**, *4*, 2058−2061.
(23) Somani, P. R.; Radhakrishnan, S. Electrochromic Materials and Devices: Present and Future. *Mater. Chem. Phys.* **2002**, *77*, 117−133.
(24) Baetens, R.; Jelle, B. P.; Gustavsen, A. Properties, Requirements and Possibilities of Smart Windows for Dynamic Daylight and Solar Energy Control in Buildings: A State-of-the-Art Review. *Sol. Energy Mater. Sol. Cells* **2010**, *94*, 87−105.
(25) Haussener, S.; Xiang, C.; Spurgeon, J. M.; Ardo, S.; Lewis, N. S.; Weber, A. Z. Modeling, Simulation, and Design Criteria for Photoelectrochemical Water-Splitting Systems. *Energy Environ. Sci.* **2012**, *5*, 9922−9935.
(26) Trotochaud, L.; Ranney, J. K.; Williams, K. N.; Boettcher, S. W. Solution-Cast Metal Oxide Thin Film Electrocatalysts for Oxygen Evolution. *J. Am. Chem. Soc.* **2012**, *134*, 17253−17261.
(27) Bendert, R. M.; Corrigan, D. A. Effect of Coprecipitated Metal Ions on the Electrochromic Properties of Nickel Hydroxide. *J. Electrochem. Soc.* **1989**, *136*, 1369−1374.
(28) Conell, R. S.; Corrigan, D. A.; Powell, B. R. The Electrochromic Properties of Sputtered Nickel Oxide Films. *Sol. Energy Mater. Sol. Cells* **1992**, *25*, 301−313.
(29) Corrigan, D. A.; Knight, S. L. Electrochemical and Spectroscopic Evidence on the Participation of Quadravalent Nickel in the Nickel Hydroxide Redox Reaction. *J. Electrochem. Soc.* **1989**, *136*, 613−619.
(30) Hall, D. E. $Ni(OH)_2$-Impregnated Anodes for Alkaline Water Electrolysis. *J. Electrochem. Soc.* **1983**, *130*, 317−321.
(31) Surendranath, Y.; Kanan, M. W.; Nocera, D. G. Mechanistic Studies of the Oxygen Evolution Reaction by a Cobalt−Phosphate Catalyst at Neutral pH. *J. Am. Chem. Soc.* **2010**, *132*, 16501−16509.
(32) Maximizing $\Phi_{o\text{-}c}$ for the photoanode catalyst does not necessarily result in a higher water-splitting efficiency in a tandem photoanode/photocathode configuration. The overall water-splitting efficiency also depends on the characteristics of the photocathode component of the device. However, in an optimized tandem device, absorber band gaps will be minimized to maximize the absorbed sunlight and hence photocurrent, which will constrain the total photovoltage available for driving water splitting. Thus, classes of catalysts with high $\Phi_{o\text{-}c}$, and therefore low parasitic optical absorption and low overpotentials, are expected to be optimal for those situations as well.